Evaluation of mast measurements and wind tunnel terrain models to describe spatially variable wind field characteristics for long-span bridge design

Tor M. Lystad[1,2*], Aksel Fenerci[2] and Ole Øiseth[2]

[1]Bridge Department, Norconsult, Sandvika, Norway

[2]Department of Structural Engineering, Norwegian University of Science and Technology, Trondheim, Norway

Abstract

The quality of the information about the wind field characteristics is crucial for accurately predicting the structural response of a long-span bridge subjected to dynamic wind loads. In this paper, in situ mast measurements and terrain model wind tunnel tests are compared with full-scale measurements of the wind field along the Hardanger Bridge girder. The aim is to investigate the performance of mast measurements and wind tunnel terrain model tests in predicting the wind field characteristics for long-span bridges in complex terrains. Wind field spatial variations and statistical distributions for the mean wind velocity and turbulence intensity are investigated. Extreme value statistics have been applied to compare the mean wind velocity recordings from two different measurement periods. Results showing terrain-induced effects on the wind directions, turbulence intensities and mean wind velocities are presented. Simultaneous spanwise wind profiles for the mean wind velocity and along-wind turbulence intensity are compared between the terrain model wind tunnel tests and the full-scale measurements, and large nonuniformities are identified. The extreme profiles of the turbulence intensities vary as much as 100% along the span, and the mean wind velocity profiles vary up to 50% along the span.

Keywords: Long-span bridge, Nonuniform wind field, Field measurements, Terrain model

1 Introduction

The Norwegian government is planning a new highway along the west coast of Norway to reduce traveling time between four of the largest cities. The Norwegian west coast is dominated by a terrain with deep fjords and tall, steep mountains, and a highway in this complex terrain demands crossing fjords as wide as 5000 m and as deep as 1300 m with fixed bridge connections. Other extreme crossings are also being proposed around the world, such as the Messina Strait and the Strait of Gibraltar, which pose large engineering challenges. The design for dynamic environmental loads is critical for such structures, and some of the methods used for the design of past bridge structures may not account for the challenges of these extreme projects.

For long-span bridges where the response from dynamic wind loading is dominating the load effects relevant for design, the quality of the information about the wind field characteristics available for the design calculations will govern the achieved structural reliability. In complex inhomogeneous terrain, the spatial variability of the statistical distributions for the wind field parameters can be large. In situ mast measurements and wind tunnel terrain model tests are currently the main approaches used to investigate the local wind field characteristics for long-span bridge design purposes. Other methods such as computational fluid dynamics (CFD) and LIDAR technology are also becoming increasingly attractive as computer performance is increasing and further development is progressing, but the traditional methods will also be important in the future. Mast measurements can be used to record the variability of the local wind field at a single point, and wind tunnel terrain model tests can be used to investigate the spatial transfer of the turbulence characteristics from the mast position to the bridge span. There are a few wind tunnel terrain model experiments for bridge design purposes presented in the literature (Hui et al., 2009a, 2009b, Li et al., 2010, 2015), but there is still a need to investigate this method's ability to spatially transfer mast measurements to the bridge span through studies comparing terrain model results with full-scale measurements, especially in complex terrain.

* Corresponding author: tor.martin.lystad@norconsult.com

Design calculations of the dynamic bridge response due to stochastic wind loads are still mainly based on the buffeting theory first introduced by (Davenport, 1962) and improved by (Scanlan, 1978a, 1978b; Scanlan and Tomko, 1971). Many full-scale bridge measurement campaigns have been performed to verify the performance of the buffeting theory (Bietry et al., 1995; Brownjohn et al., 1994; Cheynet et al., 2016; Cross et al., 2013; Fenerci et al., 2017; Fenerci and Øiseth, 2018, 2017; Macdonald, 2003; Miyata et al., 2002; Wang et al., 2011, 2013; Xu, 2013), with some campaigns finding good agreement and others finding significant discrepancies. In traditional design approaches, based on a short-term stationary and homogeneous wind field assumption, the turbulence characteristics are commonly chosen as deterministic parameters, although a significant variability in the measured wind field characteristics and bridge responses are presented in several of the referred full-scale measurement campaigns. (Fenerci et al., 2017) have shown that it is possible to account for most of the measured response scatter if detailed information about the variability in the wind field parameters is available. More advanced methods such as probabilistic design approaches (Ciampoli et al., 2011; Davenport, 1983; Kareem, 1988; Pagnini, 2010; Pagnini and Solari, 2002; Solari, 1997; Spence and Kareem, 2014; Zhang et al., 2008) or long-term extreme response analysis (Xu et al., 2017) are able to account for the variability in the load to a greater extent, but these methods rely on a more complete statistical description of the load than that used in the traditional methods. Without the bridge in place, the statistical distributions for the wind field parameters can be achieved by mast measurements close to the bridge span, but this approach will rely on the ability to spatially transfer the full statistical distributions to the bridge span.

Several studies in the literature have undertaken the long-term monitoring of turbulence characteristics, thus contributing to the understanding of wind field characteristics in different topographies. Most of the measurement campaigns have been located in typhoon- and monsoon-dominated areas, such as the work performed by (Cao et al., 2009; Choi, 1978; Li et al., 2015; Wang et al., 2017), and have consisted of full-scale bridge monitoring campaigns such as (Hu et al., 2013; Hui et al., 2009a, 2009b; Miyata et al., 2002; Wang et al., 2013, 2011, 2009, 2014). Additionally, for European conditions, many wind field characterization studies can be found in the literature (Bietry et al., 1995; Bocciolone et al., 1992; Brownjohn et al., 1994; Cheynet et al., 2016; Cross et al., 2013; Fenerci et al., 2017; Fenerci and Øiseth, 2018, 2017; Harstveit, 1996; Macdonald, 2003). Although all these studies provide valuable insights, most of them have been based on very few wind sensors (some only measured the wind field characteristics at a single point) that are unable to describe spatial variations in the wind field. (Burlando et al., 2013) address the problem of spatially transferring measured wind velocities to a target site using CFD, but on a less detailed scale than what is necessary for terrains that exhibit extreme complexity. For long-span bridge design purposes, there is still a need for studies investigating spatial variations of wind velocities and turbulence characteristics, especially in complex terrain where terrain-induced variations can be large.

In the years prior to the construction of the Hardanger Bridge, in situ mast measurements and wind tunnel terrain model tests were performed to investigate the local wind field characteristics at the bridge site. Since the opening of the bridge in 2013, the Norwegian University of Science and Technology (NTNU) has been monitoring the wind field along the bridge girder using 8 ultrasonic anemometers. This paper is an extension of the preliminary results presented at the European-African Conference on Wind Engineering in 2017 (Lystad et al., 2017). In this paper, we study the spatial variations in the statistical distributions for mean wind velocity and along-wind turbulence intensity at the Hardanger Bridge site and the performance of the traditional wind field characterization methods for describing these statistical distributions along the bridge span in complex terrain.

In section 2 the measurement campaigns used in this study are introduced, and in section 3 flow patterns at the bridge site are interpreted using wind directionality effects as basis. Section 4 investigates the spatial transfer of the mean wind velocity extreme value distributions and the probability density function of the along-wind turbulence intensity between the mast and along girder anemometers. In section 5, spanwise simultaneously measured profiles for mean wind velocity and along wind turbulence intensity from the full-scale measurements are compared with spanwise profiles identified in the wind tunnel terrain model test. Finally, in section 6 conclusions and some recommendations for the use of the investigated methods are presented.

2 Wind field measurements

The Hardanger Bridge is a suspension bridge with a main span of 1310 m, making it the longest bridge span in Norway. The bridge crosses the Hardanger fjord, which is located in complex terrain surrounded by high, steep mountains. The surrounding terrain is extreme, but it is typical for the fjord landscape along the coastline of Norway.

2.1 Full-scale monitoring campaign

After the bridge was opened to the public in 2013, it was instrumented with a state-of-the-art monitoring system measuring wind field characteristics and acceleration responses along the bridge girder. The monitoring system consists of 20 triaxial accelerometers and 9 ultrasonic triaxial anemometers, of which 8 are distributed along the span. An overview of the wind monitoring system is shown in Fig. 2, and the system is described in more detail in (Fenerci et al., 2017).

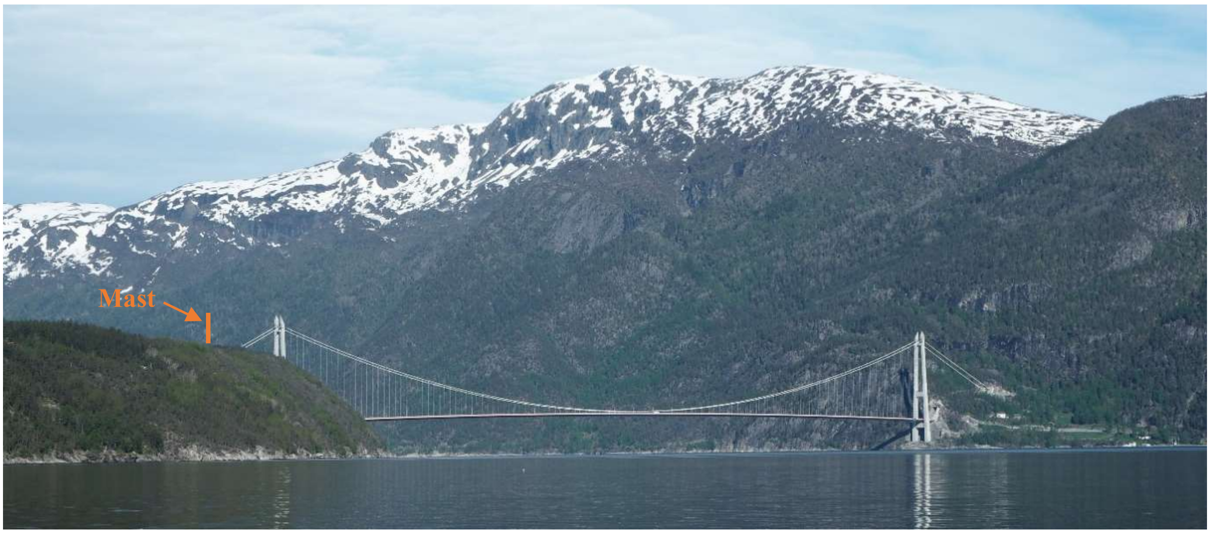

Fig. 1. The Hardanger Bridge (image by the authors)

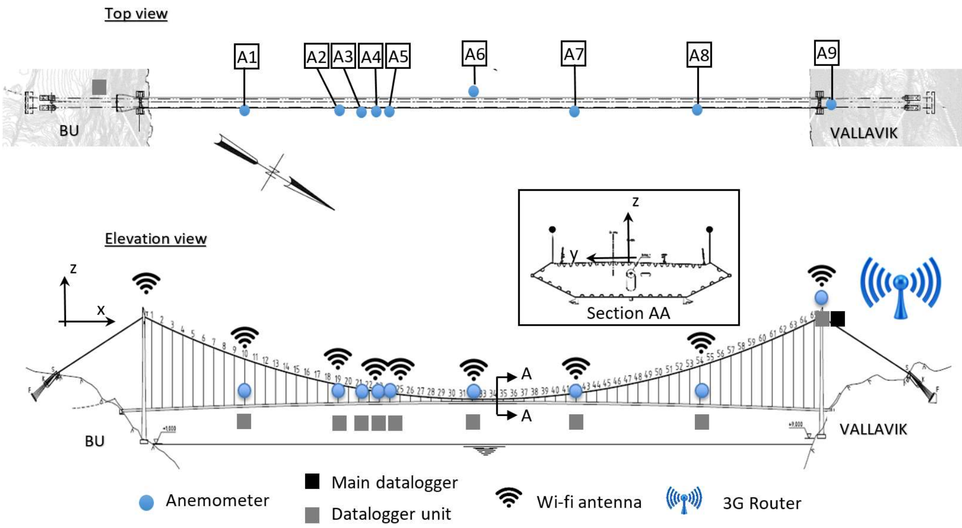

Fig. 2. Full-scale wind field measurement sensor layout

2.2 Mast measurements

During 1988-1992, the Norwegian Meteorological Institute placed a wind measurement mast on the headland Buneset, close to the southern end of the bridge, to measure the local wind field characteristics for the design of the Hardanger Bridge. Buneset is a headland extending into the fjord with an elevation of 110-130 m above mean sea level. As this headland is relatively flat and the surroundings are steep and complex, Buneset was a suitable position for the mast placement. Fig. 1 shows Buneset on the left in the picture (south), and Fig. 3 shows a picture of the bridge taken from the headland. The mast was instrumented with wind sensors at three levels, 10 m, 30 m and 45 m above ground. The results from the mast measurements are reported by (Harstveit, 1994) and discussed further by (Harstveit, 1996). In (Harstveit, 1994), it was concluded that the sensors at the two lowest levels were disturbed by the forest vegetation on the headland, so the results from these sensors were discarded. They noted that some disturbance may also be present for the 45 m sensor, affecting both the recorded turbulence intensity and the mean wind velocity. The results from the 45 m sensor were used for the design of the Hardanger Bridge, and these results are also used in the present study.

The elevation of the highest sensor (approximately 155-175 m above mean sea level) is also a concern for representing the wind field characteristics along the bridge girder (60 m above mean sea level). The effects of relative elevation, wind speed-ups as the wind flows over the headland, and differences in surface roughness are important factors for the spatial transfer of the wind field characteristics from the mast to the bridge girder.

Fig. 3. Southern tower viewed from the Buneset headland (image by the authors)

2.3 Terrain model tests

To quantify the wind field differences between the mast position and the bridge girder and to investigate the spanwise effects such as wind field profiles and covariance, a 1:2000 scale terraced terrain model of the Hardanger Bridge surroundings was tested in the boundary layer wind tunnel at NTNU. The tests were performed by the Department of Energy and Process Engineering at NTNU in 1991, and the results were reported by (Sætran and Malvik, 1991). The boundary layer wind tunnel at NTNU is a closed-circuit wind tunnel with a test section that is 11 m long, 2.7 m wide and 1.8 m high with a maximum wind speed of 30 m/s. Hot-wire anemometers were used in the experiments to measure the along-wind component of the fluctuating wind field.

The scale of 1:2000 is larger than the acceptable minimum scale for accurate modeling of the surface flow behavior, suggested by (Bowen, 2003) to be in the range of 1:2500-5000. However, (Bowen, 2003) also concluded that for terrain model scales smaller than 1:500, the accuracy of the modeled flow may be significantly reduced. Some studies investigated the surface modeling of such wind tunnel terrain models (Meroney, 1980; Stevenson et al., 1981) and concluded that special attention should be given to the effect of the surface of the model. However, both referenced studies were performed at very small scales, 1:5000 and 1:4000, respectively, which might have affected the surface modeling sensitivity. The terrain model for the Hardanger Bridge was built as a terraced model with 10 mm thick layers and no further surface roughness adjustments.

A terrain model with two main wind directions identified by the mast measurements was tested in the wind tunnel. A map cutout of these two modeled directions is shown in Fig. 4. From the bridge location, the Norwegian coastline is to the west and the inland area is to the east. (Meroney, 1980) concluded that the inflow conditions were an important aspect in modeling the local wind flow in complex terrain. For the easterly winds, two different incoming flow cases were tested to investigate the inflow effect on the locally generated wind field. The easterly winds travel over a mountainous region before hitting the bridge site, so the terrain model was subjected to both a smooth incoming flow and a turbulent incoming flow generated with a turbulence grid. However, the westerly winds, coming from the sea, were tested only with smooth inflow conditions, as the local terrain was expected to generate most of the turbulence effects. For all the tests, an incoming wind velocity of 16 m/s was used in the wind tunnel.

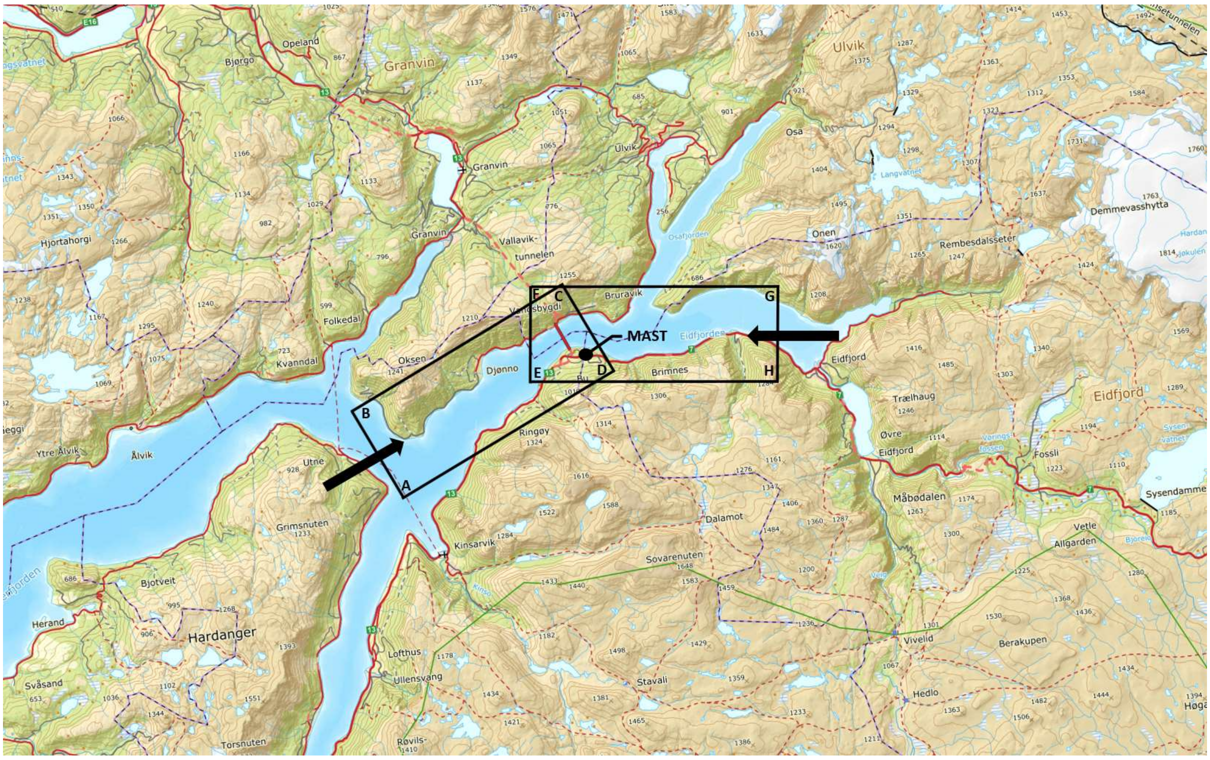

Fig. 4. Terrain model map cutout. ABCD represent westerly winds, and EFGH represent easterly winds (map from Kartverket©; the shown area is approximately 25x40 km at full-scale)

3 Effects of wind direction

The directional wind field characteristics measured by the mast are compared with the recorded wind field along the bridge girder from the bridge monitoring campaign in Figs. 5 and 6. The monitoring system anemometers are distributed along the bridge girder, from A1 at the south end to A8 at the north end of the bridge. The mast position is close to the south end of the bridge, so the A1 sensor is the anemometer closest to the mast position.

The strong wind roses shown in Fig. 5 display percentages of the amount of strong wind measurements (> 15 m/s) only, and not the total amount of expected wind recordings during the measurement period. It can be observed that the percentage of winds above 18 m/s is larger for the westerly winds than the easterly winds. Considering the westerly winds, the recorded mean wind direction changes slightly towards the midspan coming more directly from the west. Terrain-induced channeling effects become clearer towards each bridge end, where the recorded mean wind is following the southwesterly fjord direction. A possible flow pattern that could explain this behavior is that the dominant incoming wind direction is more directly westerly, but the fjord direction is locally channeling the wind direction at the bridge site. The flow measured at the southern part of the span will then travel a longer distance along the fjord than the wind closer to the midspan, being more strongly affected by the channeling effects. This characteristic flow pattern is illustrated in Fig. 6a. (Harstveit, 1994) also indicated a similar flow pattern for the westerly winds, although focusing on the flow over the Buneset headland rather than the along-span behavior. In the northern part of the span, the steep mountainside to the northwest of the bridge is greatly affecting the wind field, and the measured wind directions suggest strong channeling effects at this part of the bridge span.

Towards the east of the bridge, the fjord split into two fjord arms, which causes an interesting spanwise wind field behavior. The dominating winds hitting the southern part of the bridge span, A1-A6, are coming from the southern fjord arm, but towards the northern part of the bridge span, A7-A8, the dominating winds are increasingly coming from the northern fjord arm. Thus, the wind field coming from the east seems to be composed of two different incoming flows channeled by the two fjord arms. The assumed easterly wind flow pattern is illustrated in Fig. 6b.

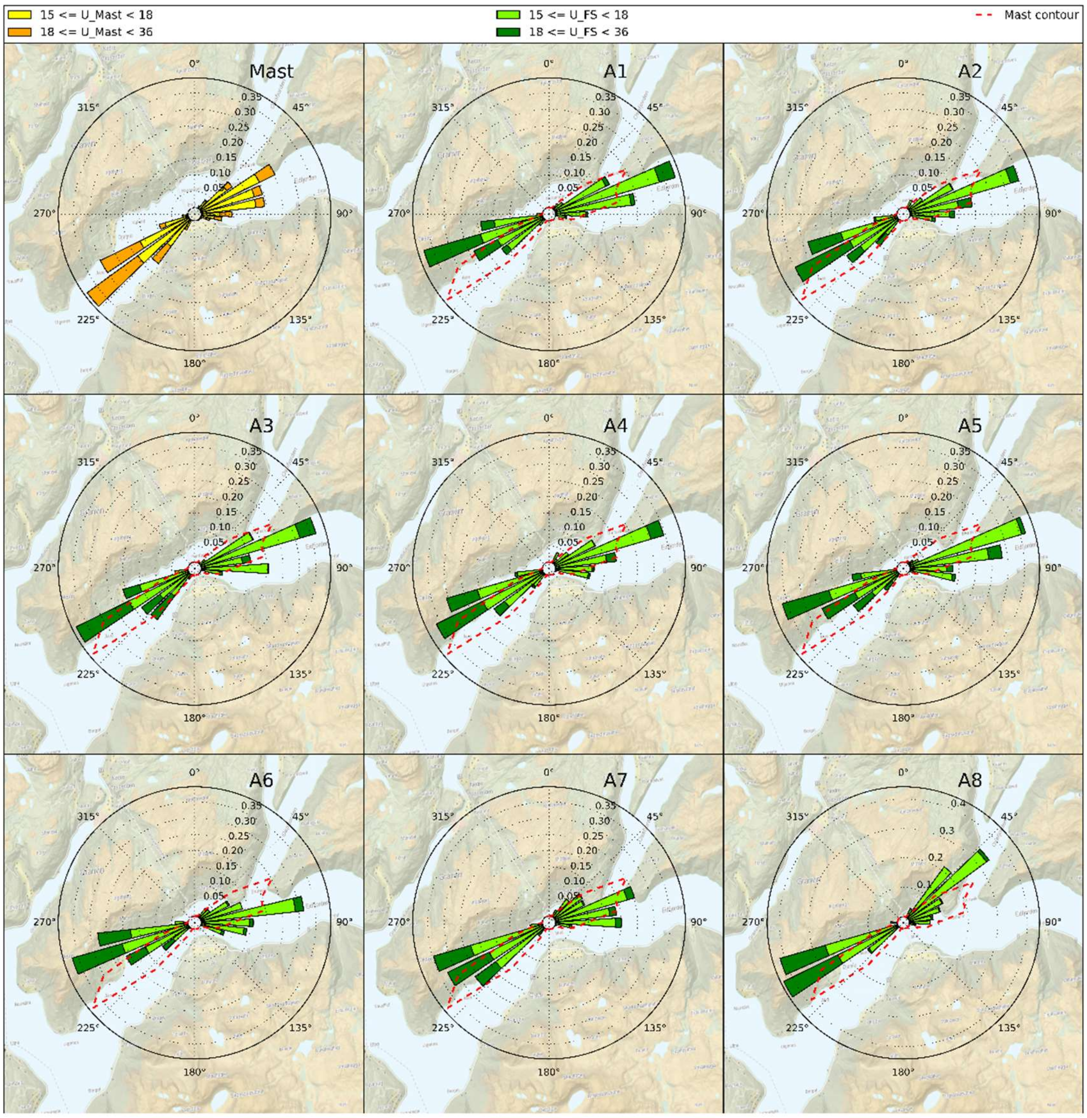

Fig. 5. Mean wind velocity wind roses. The wind roses present percentages of strong winds above 15 m/s only, and are divided into two main wind directions, east and west, with each side adding up to 100% (background from Kartverket©)

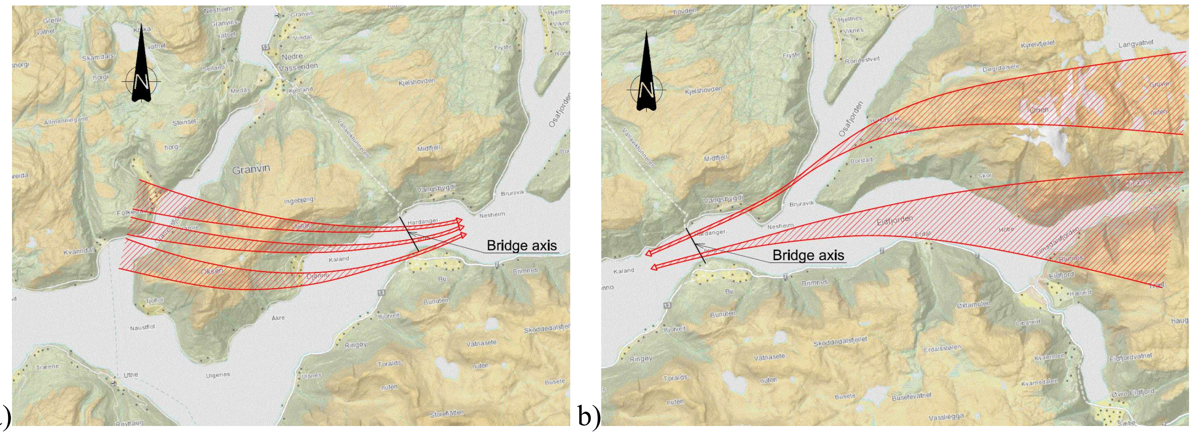

Fig. 6. Characteristic flow pattern; a) westerly winds and b) easterly winds (map from Kartverket©)

In Fig. 7, the turbulence intensity wind roses are plotted for the mast measurements and the anemometers distributed along the girder. Only strong winds with mean wind velocities above 10 m/s are presented. For the westerly winds, we observe an increasing turbulence intensity from the southern to the northern part of the span. The very steep mountainside to the northwest of the bridge is increasingly affecting the westerly wind turbulence towards the north. This behavior is also supporting the assumed flow pattern shown in Fig. 6a, where the westerly winds are coming down this steep mountain before hitting the bridge span. For the easterly winds, the turbulence intensity distribution is more uniform. Based on the observation made in the previous section, that the easterly wind field is composed of two different incoming flows, a larger variation in the turbulence characteristics along the span could be expected, but it seems the two fjord arms are generating a similar wind field.

Comparing the turbulence characteristics towards the southern part of the span with the mast measurements, larger percentages of high turbulence intensities are observed for the mast measurements than for the anemometers along the girder. This observation is discussed further in the following sections.

It should be noted that the full-scale measurement system is set with an automatic trigger for recordings where one of the anemometers measures a mean wind velocity above 15 m/s. Since a mean wind velocity over the trigger threshold only needs to be measured by one anemometer and due to manually triggered periods, a significant number of measurements between 10 and 15 m/s are still present, although the full distribution is not available in this range. The raw data from the mast measurement results are not available, so the previously binned results presented by (Harstveit, 1994) are used in this study. The available mast turbulence intensities are binned for mean wind velocities above 10 m/s, and not 15 m/s, so for comparison reasons, the same range of mean wind velocities are chosen for the anemometers along the girder.

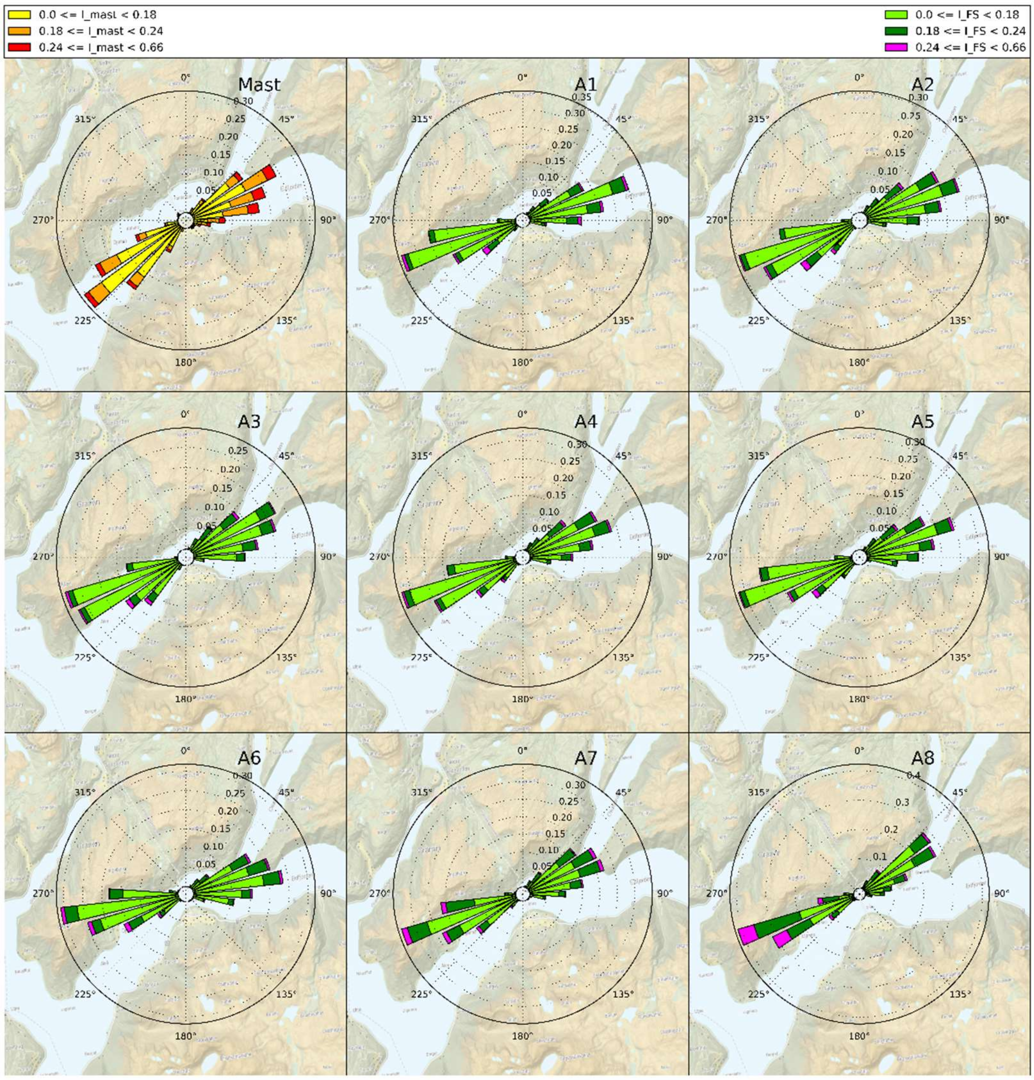

Fig. 7. Turbulence intensity wind roses. The wind roses are divided into two main wind directions, east and west, with each side adding up to 100% (background from Kartverket©)

4 Spatial transfer of wind field characteristics

In situ mast measurements are the most commonly used source of information about the wind field characteristics for the design of long-span bridges. In this section, the performance of the mast measurements in predicting wind field characteristics along the Hardanger Bridge girder is investigated. The results from the four-year mast measurement campaign are compared with the results from four years of along-girder measurements performed by NTNU. Extreme wind speeds and turbulence intensities are considered, and spatial transfer coefficients between the mast and the positions along the girder are estimated. The spatial transfer coefficients are defined here as the ratio between mast measurements and along span anemometers and will be further discussed in the following sections.

4.1 Extreme value statistics

The mean wind velocity is the most important parameter when predicting the aerodynamic response of a long-span bridge. To create a spatial transfer coefficient for the mean wind velocity between nonsimultaneous recordings from the mast and the along-span anemometers, extreme value distrubutions for the mean wind speed are considered, utilizing the Method of Independent Storms (MIS). The background theory of this method and other recent developments in the field of extreme value statistics are presented in the following paragraphs.

If the parent probability distribution of a stochastic variable is of the exponential type, which is the case for the commonly used Weibull distribution for the mean wind velocity, it can be shown that the asymptotic extreme value distribution will follow a type I generalized extreme value (GEV) distribution form (Gumbel distribution). The general parent cumulative probability distribution form of the exponential type can be written as

$$P_X(x) = 1 - e^{-h(x)} \tag{1}$$

and the type I generalized extreme value cumulative probability distribution can be written as

$$P_Z(z) = 1 - e^{-e^{-y}}, \quad y = (z-u)/\beta \tag{2}$$

where u and β are the location and scale parameters of the distribution, respectively, and y is the reduced variate. The relationship between the parent distribution, $P_X(x)$, and the asymptotic extreme value distribution, $P_Z(x)$, is expressed below, given that the values of x drawn from the parent distribution are statistically independent and that N is the number of independent storm extreme values drawn from the parent distribution.

$$P_Z(x) = [P_X(x)]^N \tag{3}$$

For the asymptotic limit where $N \rightarrow \infty$, the extreme value distribution approaches the GEV distribution. The original Gumbel method presented by (Gumbel, 1958) for estimating the extreme value distribution takes advantage of the known shape of the distribution, assuming a type I GEV distribution form. Since the reduced variate y is a linear function for the type I distribution, the Gumbel method estimated the order statistics, u and β, by fitting a straight line to the measurements using linear regression. The reduced variate y can be expressed as follows, using the type I GEV form:

$$y = -\ln[-\ln(P_Z(z))] \tag{4}$$

To obtain realizations of y from the recordings, the extreme value probability $P_Z(z)$ must be calculated for each recording. This can be achieved by ranking the annual extreme value recordings in ascending order giving the lowest recorded annual extreme the rank of $m=1$ and the highest annual extreme the rank of $m=n$, where n is the total number of recorded annual extremes. Then, the non-exceedance extreme value probability of each annual maximum can be calculated from these ranks:

$$P_Z(z) = m/(n+1) \tag{5}$$

The linear regression approach suggested by (Gumbel, 1958) was further investigated by (Lieblein, 1974), who proposed an adjusted method using tabulated coefficients to avoid biased estimates for the order statistics from the fitted curve for the reduced variate. This approach is referred to as the Gumbel-Lieblein BLUE (best linear unbiased estimator) method and was tabulated for up to 16 extreme value recordings by (Lieblein, 1974), and increased to 30 values by (Balakrishnan and Chan, 1992). (Harris, 1996) further generalized the Gumbel-Lieblein BLUE method introducing a new minimum-variance bias free procedure and suggested that the axes in the traditional Gumbel plot should be interchanged. (Harris, 1996) also suggested that for extreme wind velocities, a better estimation of the extreme value distribution due to a faster convergence rate was achieved by fitting the square of the mean wind velocity $q=U^2$ to the reduced variate y, an approach also used in the Eurocode (Tamura and Kareem, 2013).

For the general Gumbel-Lieblein BLUE method, only recorded yearly maxima are used to fit the extreme value distribution. This approach demands a very long measurement period to give reliable estimates for the extreme value distribution. However, (Cook, 1982) proposed a modified approach taking advantage of more than one extreme recording a year, given that the recorded extreme values are statistically independent, known as the Method of Independent Storms (MIS). By introducing the parameter r for the annual rate of independent storms, the following relationship was proposed:

$$r = n_s / T_s \tag{6}$$

where n_s is the number of independent storm extreme values used in the calculations and T_s is the measurement period in years. Then, the annual extreme value distribution can be expressed as:

$$P_Z(z) = [P_{Z-s}(z)]^r = [m_s / (n_s + 1)]^r \tag{7}$$

where $P_{Z\text{-}s}(z)$ is the individual storms extreme value distribution, m_s is the individual storm rank and $P_Z(z)$ is the annual extreme value distribution. In this way the number of extremes available for practical purposes could be significantly improved. (Cook, 1982) also introduced a method for using the Gumbel-Liebline BLUE approach utilizing more extreme values than the tabulated coefficients from the method would suggest, but a better estimate based on a larger number of extreme values was achieved using Harris' method (Harris, 1999). Recent development in the field of extreme value characterization has shown that using the asymptotic extreme value distribution methods described above may lead to significant discrepancies for the estimation of extreme wind speeds with large return periods (Ian Harris, 2014; Torrielli et al., 2013). Penultimate distribution methods arguing that the number of extremes used, rT_s, is too low to justify an asymptotic assumption where $rT_s \to \infty$ are also presented in the literature (Cook and Harris, 2008, 2004; Harris, 2009) showing better performance for large return periods up to 10 000 years.

In the following investigations, the MIS method based on the Gumbel-Lieblein BLUE approach is used. Other methods may provide better estimates of the extrapolated large return period extreme wind speeds, but they will rely on a larger number of extremes than that available from the mast measurements in (Harstveit, 1994) to improve the performance compared to the MIS approach. However, for the sake of comparison between nonsimultaneous wind recordings in this study the chosen methodology is deemed satisfactory.

4.2 Mean wind velocity

By applying the individual storms approach and the Gumbel-Lieblein BLUE method, a mean wind velocity extreme value distribution for the mast measurements and the anemometers along the bridge girder was fitted based on the 16 largest statistically independent individual storms during the four-year measuring periods. As noted by Kasperski in (Tamura and Kareem, 2013), the common practice to ensure statistical independence among the recorded individual storm maxima is to require a low mean wind speed over a longer period of 12-24 h, since a single storm may calm down before strengthening again. In the present study, the criterion described by Kasperski was followed, demanding a minimum of 12 h of winds below 15 m/s between the individual storms. However, for the mast measurements, the criterion set to identify statistically independent storms was that the mean wind velocity should fall below 10 m/s between each recorded storm maxima. Although this criterion may principally lead to maxima from the same storm, the time of the measured extreme values are known, and well separated, so the individual storms can also be determined as statistically independent for the mast recordings. The measurements were divided into the two main wind directions, considering westerly and easterly winds separately.

The location of the mast on top of the Buneset headland suggests that wind speed-up effects due to local topography may affect the mean wind velocity, as investigated by (Carpenter and Locke, 1999; Miller and Davenport, 1998). In the European design code for wind actions (Standard Norge, 2009), speed-up effects due to flow over local hill tops can be defined by the terrain shape factor c_o, also referred to as the speed-up ratio in the literature (Miller and Davenport, 1998; Stevenson et al., 1981; Tamura and Kareem, 2013):

$$c_o = v_m / v_{mf} \tag{8}$$

where v_m is the increased wind velocity due to speed-up effects and v_{mf} is the reference velocity.

For the design of the Hardanger Bridge, the terrain model wind tunnel tests were used to estimate the spatial transfer coefficient, or speed-up ratio as defined in Eq. (8), between the mast position and the midspan of the bridge. For the westerly winds, they concluded that the midspan girder wind speed was only 6% lower than the wind speed measured by the mast. For the easterly winds, the measured midspan wind speed was 20% lower than the wind speed in the mast position for the smooth inflow case and 15% lower than that for the turbulent inflow case. Since the strongest winds were measured coming from the west and the wind tunnel tests showed a low difference in the wind velocity between the mast and the girder midspan for this direction, no reduction in the measured mast wind velocities were used in the design.

In Figs. 8 and 9, fitted Gumbel-Lieblein plots are shown for the easterly and westerly winds, respectively, comparing the extreme winds measured by the mast with the along-girder anemometers. The fitted curves are not linear in the plots because the line is fitted to the square of the mean wind velocity and plotted against the linear mean wind velocity axis. In Fig. 10, the fitted extreme value probability distribution is plotted along the bridge span through a contour plot for both easterly and westerly winds. The mean wind velocity, with a statistical return period of 2 and 50 years, is indicated for the along-span variation and the mast extreme wind velocities. In Tables 1 and 2, extreme winds for 2 and 50 year statistical return periods are shown for all sensors, as well as the speed-up ratio for the mast using measurements along the bridge girder as reference wind speeds.

It can be observed that the mast measurements overestimate the wind speed compared with the positions along the girder for both wind directions. Comparing the midspan (A6) speed-up ratios observed from the full-scale measurements with the predicted coefficients from the terrain model wind tunnel test results c, a good estimate for the easterly winds can be observed, but for the westerly winds, the terrain model experiments show a significantly lower speed-up ratio than that observed from the full-scale measurements. This may be explained by observing the difference in wind directions for the westerly winds between the mast measurements and the midspan anemometer, A6, and the assumed flow pattern shown in Fig. 7a. As the westerly direction modelled in the wind tunnel may be slightly inaccurate for the dominating winds, as discussed in the previous sections, important information about the local flow over the Buneset headland may have been lost resulting in an underestimated speed-up ratio.

The European design code for wind actions (Standard Norge, 2009) gives guidelines for calculating local variations in the wind velocity based on the inclination of the upstream hill and the position relative to the hill. The relationship for an inclination ratio of $\Phi=H/L_u > 0.3$ is defined as follows

$$c_o = 1 + 0.6s \tag{9}$$

where s is a factor accounting for the position relative to the hill and the terrain shape. It should be noted that the guidelines given in the Eurocode are not valid for complex terrain such as the Hardanger Bridge site, but it is interesting to see how well the guidelines can perform also under such conditions. A good performance may indicate isolated effects, less influenced by the surrounding terrain complexity. By applying the calculation procedure for local wind speed-ups over a single hill proposed in the design codes, a speed-up ratio of 1.24 for the easterly winds and 1.18 for the westerly winds can be determined, corresponding very well with the observed speed-up ratios from the full-scale measurements in Tables 1 and 2. In this calculation, $\Phi=0.33$ and $s=0.4$ were used for the easterly winds, and $\Phi=0.5$ and $s=0.3$ were used for the westerly winds, based on the mast distance from the upstream hill and the steepness of the hill.

For the easterly extreme wind velocity distribution plotted in Fig. 10a, a uniform distribution along the span is shown, although slight reductions towards the ends are visible. The same trend can be observed for the westerly wind direction in Fig. 10b, although stronger reductions towards the ends are present. Additionally, a weak linear trend from the A8 sensor in the north to the A5 sensor can be observed for the westerly winds.

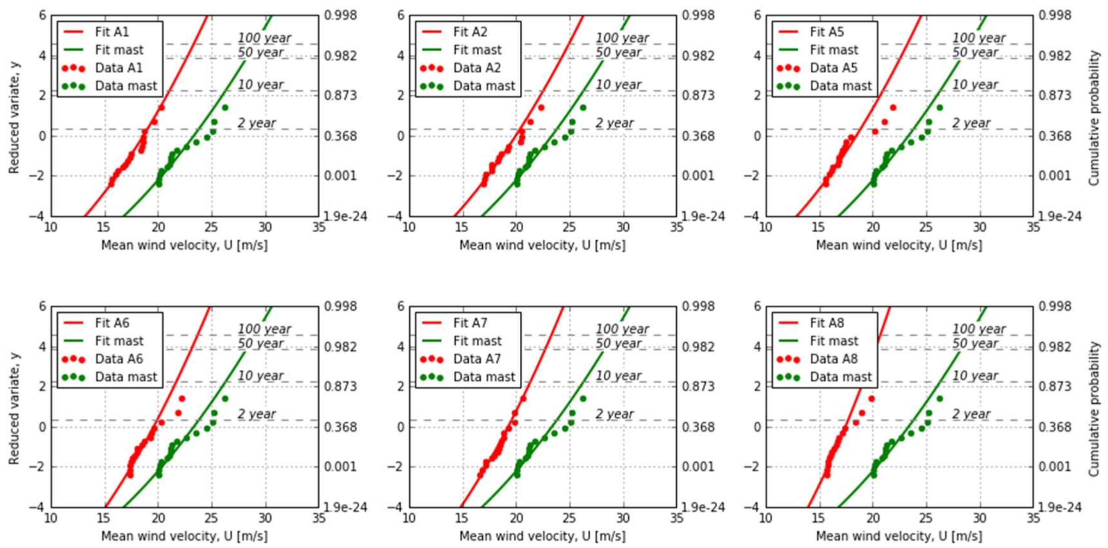

Fig. 8. Gumbel-Lieblein plots for the extreme mean wind velocities of chosen anemometers for easterly winds

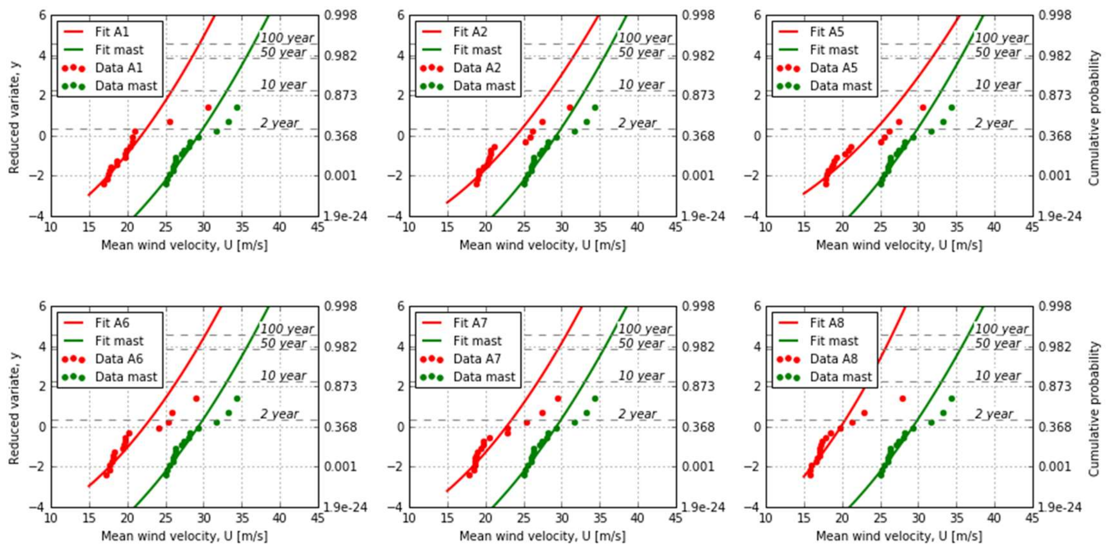

Fig. 9. Gumbel-Lieblein plots for the extreme mean wind velocities of chosen anemometers for westerly winds

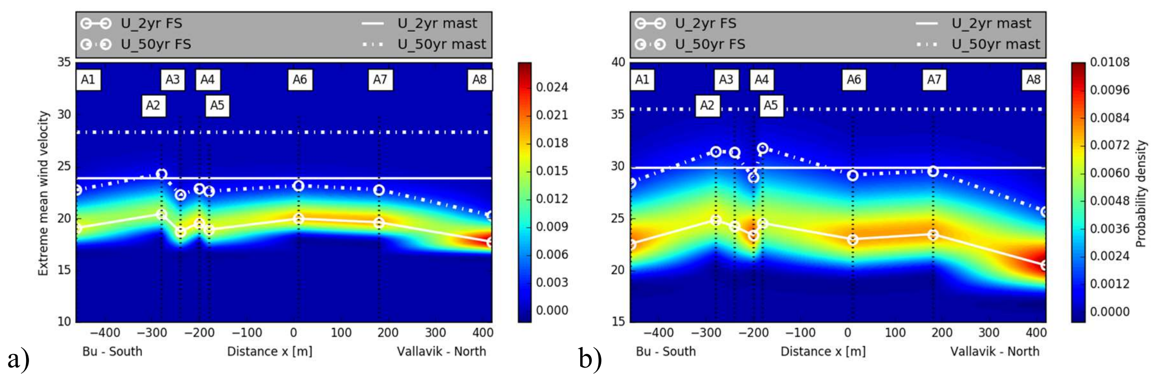

Fig. 10. Extreme value probability density for the mean wind velocity of a) easterly winds and b) westerly winds

Sensor	x [m]	U_{2yr}	U_{10yr}	U_{50yr}	U_{100yr}	$c_{o,2yr}$	$c_{o,50yr}$
Mast	~1000	23.9	26.4	28.3	29.1	1	1
A1	460	19.1	21.1	22.7	23.4	1.25	1.25
A2	280	20.4	22.6	24.3	25.0	1.17	1.17
A3	240	18.8	20.7	22.3	22.9	1.27	1.27
A4	200	19.6	21.4	22.9	23.5	1.22	1.24
A5	180	18.9	21.0	22.6	23.3	1.26	1.25
A6	-10	20.0	21.7	23.2	23.8	1.20	1.22
A7	-180	19.6	21.4	22.8	23.4	1.22	1.24
A8	-420	17.7	19.1	20.3	20.7	1.35	1.40
Eurocode	-	-	-	-	-	1.24	
Terrain model	-	-	-	-	-	1.20/1.15	

Table 1. Mean wind velocity extreme values and speed-up ratios for the easterly winds

Sensor	x [m]	U_{2yr}	U_{10yr}	U_{50yr}	U_{100yr}	$c_{o,2yr}$	$c_{o,50yr}$
Mast	~1000	30.0	33.1	35.6	36.6	1	1
A1	460	22.6	25.9	28.5	29.5	1.33	1.25
A2	280	24.8	28.6	31.5	32.6	1.21	1.13
A3	240	24.3	28.3	31.4	32.6	1.23	1.13
A4	200	23.4	26.5	29.0	29.9	1.28	1.23
A5	180	24.6	28.7	31.8	33.1	1.22	1.12
A6	-10	23.0	26.5	29.2	30.3	1.30	1.22
A7	-180	23.5	26.9	29.6	30.6	1.27	1.20
A8	-420	20.5	23.4	25.7	26.6	1.46	1.38
Eurocode	-	-	-	-	-	1.18	
Terrain model	-	-	-	-	-	1.06	

Table 2. Mean wind velocity extreme values and speed-up ratios for the westerly winds

In this section, the extreme value statistics have been used to compare recordings from two different measurement periods. Some caution should be used due to possible biased differences between the two periods. There are no long-term wind measurement stations very close to the bridge site that cover both periods, as they are 25 years apart, but a qualitative comparison of the monthly maxima from a measuring station in the same area have been performed without any observed significant differences in the wind velocities. Additionally, the measurement periods of 4 years are relatively long, so a good statistical foundation can be expected, thus adding to the validation of the results.

4.3 Turbulence intensity

The turbulence intensity is another one of the most important wind field characteristics for design of long-span bridges, especially when dealing with buffeting response. Aerodynamic effects such as vortex induced vibrations (VIV) and aeroelastic instability phenomena are also affected by turbulence, however VIV is more critical for lower wind speeds and aeroelastic instability is, or at least should be, critical for higher wind speeds than what is considered in this study. Thus, based on the turbulent wind recordings considered here, the discussion in the following will be related to buffeting effects for long-span bridges. In situ mast measurements are one of the main sources of information about the local turbulence content of the wind field for the design of long-span bridges. In complex terrain, the turbulent wind field can be expected to have large terrain-induced spatial variations, as observed by (Li et al., 2010, 2016). Hence, the positioning of the measurement mast and the physical interpretation of its ability to represent the along-span turbulent wind field characteristics can be very important. In this section, the along-wind turbulence intensity statistical distributions are investigated. The along-wind turbulence intensity is defined as follows:

$$I_u = \sigma_u / U \tag{10}$$

where σ_u is the standard deviation of the fluctuating wind process and U is the mean wind velocity.

The expected value and the variability of the turbulence intensity from the bridge monitoring recordings are compared with the mast measurements. Strong wind recordings with a mean wind velocity above 10 m/s are considered, and again, the wind field is divided into the two dominating directions, easterly and westerly winds, as they display a different behavior. In Figs. 11 and 12, histogram plots of the turbulence intensities along the bridge span are shown together with fitted log-normal probability density functions (PDFs). The fitted PDFs from the mast measurements are indicated in all figures for comparison purposes. The fitted PDF for the strong wind turbulence intensity follows the log-normal distribution very well both for the along-span anemometers and for the mast measurements. In Fig. 13, a contour plot of the PDF for the along-wind turbulence intensity is plotted along the span. The expected value and the 95th percentile of the turbulence intensity are indicated in the same figure. In Tables 3 and 4, the turbulence intensity expected values, standard deviations and 95th percentiles, and the spatial transfer coefficients for these statistical parameters between the mast and the along-span anemometers are presented. The spatial transfer coefficients are defined as the ratio between the statistical distribution at the mast position (noted *mast*) and the along-span anemometers (noted *anemo*) as

$$\gamma_{stat} = I_{stat,mast} / I_{stat,anemo} \tag{11}$$

where $I_{stat,mast}$ and $I_{stat,anemo}$ can be any statistical entry such as the mean value, standard deviation or 95th percentile of the along-wind turbulence intensity.

Considering the easterly winds, the turbulence intensity is uniformly distributed along the span, both in mean value and variability. Comparing the along-span anemometers with the mast measurements, Table 3 shows that the mast measurements overestimate the mean value by 14% and the 95th percentile by 23% for the midspan sensor A6. Thus, the error made by using the mast measurements directly would, in this case, become larger for a probabilistic design approach than if the design was based on the expected value as a deterministic parameter.

A similar trend can be observed for the westerly winds, where both the mean and variability are larger in the mast measurements than in the along-span anemometers close to the southern bridge end. These observations indicate that the mast measurement turbulence intensities may be affected by the forest vegetation surrounding the mast, as noted and commented upon in the mast report (Harstveit, 1994). European design codes for wind actions (Standard Norge, 2009) state that the standard deviation of the fluctuating wind process should be unchanged by the terrain form creating the speed-up effects discussed in the previous section. Therefore, by increasing the mean wind velocity and keeping the standard deviation of the process unchanged, the turbulence intensity decreases. However, (Miller and Davenport, 1998) made observations contradictory to this effect and concluded that the design codes would yield unconservative values for turbulence intensities following these guidelines. Although the surface roughness due to the local forest vegetation on Buneset can explain at least parts of the overestimated turbulence intensities, flow separation effects due to the flow over the headland may also be present, in accordance with the observations made by (Miller and Davenport, 1998). S. Cao also concluded in (Tamura and Kareem, 2013) that flow separation may occur over hilltops when the upstream slope is larger than 17°, which is the case for both wind directions at Buneset.

Another factor that may affect the difference among the turbulence intensity distributions is the incomplete conditional distribution for the wind speeds between 10 and 15 m/s for the bridge monitoring measurements, due to the triggering threshold previously discussed in section 3. However, as shown by (Fenerci and Øiseth, 2017), the conditional turbulence intensity distribution for mean wind velocities in the range of 10–15 m/s is similar to the range of 15–20 m/s for the Hardanger Bridge, and since the error is only connected to the weight of the contributions from this range, this effect is not expected to significantly influence the results.

An interesting behavior can be observed for the westerly winds where the turbulence intensity distributions are changing significantly along the bridge span, showing a very nonuniform behavior in both mean value and variability. The expected value for the turbulence intensity is increasing from south to north by as much as 50%, and the mast measurements change from overestimating the turbulence intensity in the southern part of the span to underestimating it in the northern part. This effect was also indicated in Fig. 7, where high turbulence intensities were observed towards the A8 sensor for westerly winds generated by the mountain to the northwest of the bridge.

It is also noted that the fitted lognormal distributions are following the turbulence intensity histograms very well for all the along-span anemometers. The histograms for the mast measurements are sorted in wider bins due to the available datasets, but a lognormal distribution still follows the distribution well. The lognormal probability density function can be written as

$$f(x) = \frac{1}{x\sigma\sqrt{2\pi}} e^{\left\{\frac{-(\ln x-\mu)^2}{2\sigma^2}\right\}}; x > 0 \tag{12}$$

where μ (the mean of the natural logarithm of the random variable) and σ (the standard deviation of the natural logarithm of the random variable) are the distribution parameters. The fitted distribution parameters for the turbulence intensities are shown in Tables 3 and 4.

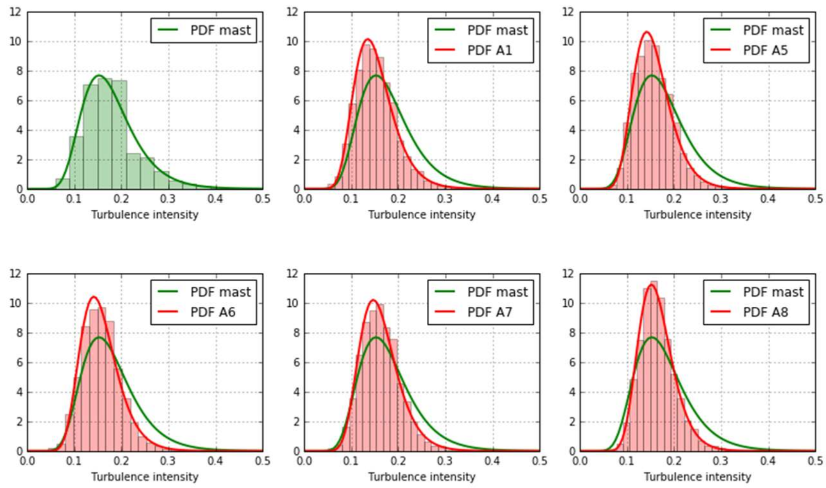

Fig. 11. Fitted probability density functions of chosen anemometers for the easterly along-wind turbulence intensities

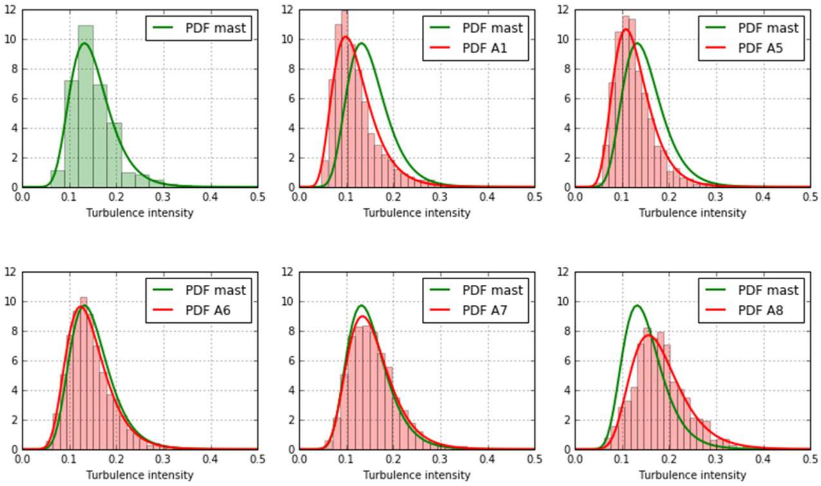

Fig. 12. Fitted probability density functions of chosen anemometers for the westerly along-wind turbulence intensities

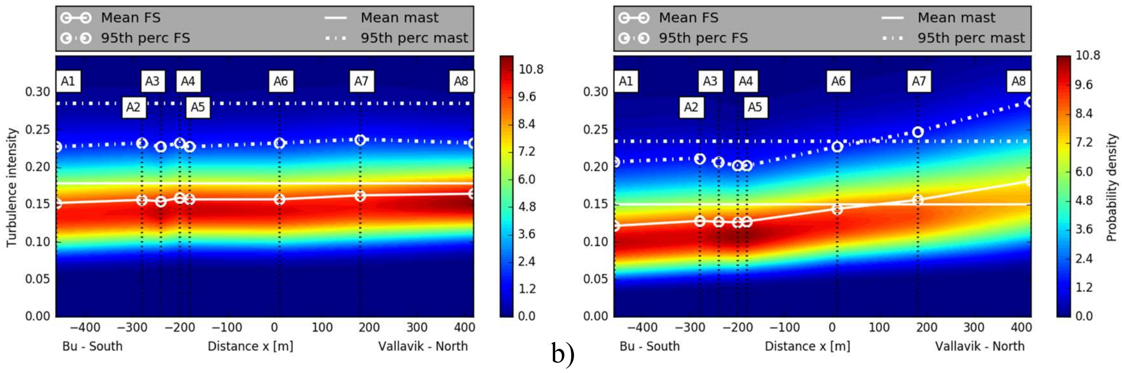

a) b)

Fig. 13. Probability density distributions for the along-wind turbulence intensity I_u of the a) easterly winds and b) westerly winds

Sensor	x [m]	Mean	Std	95th	γ_{mean}	γ_{std}	γ_{95th}	μ	σ
ast	~1000	0.179	0.059	0.286	1	1	1	-1.722	0.322
A1	460	0.152	0.043	0.227	1.17	1.36	1.26	-1.883	0.279
A2	280	0.156	0.042	0.232	1.14	1.39	1.23	-1.856	0.266
A3	240	0.155	0.040	0.227	1.16	1.47	1.26	-1.868	0.256
A4	200	0.159	0.042	0.232	1.12	1.40	1.23	-1.840	0.260
A5	180	0.157	0.041	0.227	1.14	1.45	1.26	-1.852	0.254
A6	-10	0.157	0.042	0.232	1.14	1.42	1.23	-1.851	0.260
A7	-180	0.162	0.042	0.237	1.10	1.39	1.20	-1.818	0.256
A8	-420	0.165	0.038	0.232	1.09	1.56	1.23	-1.805	0.226

Table 3. Turbulence intensity statistics and spatial transfer coefficients for the easterly winds

Sensor	x [m]	Mean	Std	95^{th}	γ_{mean}	γ_{std}	γ_{95th}	μ	σ
Mast	~1000	0.151	0.046	0.235	1	1	1	-1.889	0.295
A1	460	0.122	0.046	0.207	1.24	0.98	1.14	-2.107	0.369
A2	280	0.128	0.046	0.212	1.18	0.98	1.11	-2.053	0.351
A3	240	0.127	0.044	0.207	1.19	1.04	1.14	-2.062	0.336
A4	200	0.126	0.043	0.202	1.20	1.06	1.16	-2.068	0.331
A5	180	0.128	0.043	0.202	1.19	1.07	1.16	-2.059	0.325
A6	-10	0.144	0.047	0.227	1.05	0.98	1.03	-1.935	0.316
A7	-180	0.156	0.050	0.247	0.97	0.91	0.95	-1.857	0.313
A8	-420	0.182	0.059	0.288	0.83	0.78	0.82	-1.705	0.314

Table 4. Turbulence intensity statistics and spatial transfer coefficients for the westerly winds

5 Spanwise wind profiles

The wind field characteristics at the Hardanger Bridge site show large spatial variability along the span, especially for the turbulence intensity, as shown in the previous sections. The terrain model wind tunnel tests of the Hardanger Bridge site were used to investigate such terrain-induced spatial variations in the wind field.

In this section, simultaneously measured full-scale wind profiles along the bridge girder are shown for mean wind velocities and along-wind turbulence intensities and compared with the wind profiles measured in the wind tunnel. Only strong winds are considered with a midspan mean wind velocity above 12 m/s.

The full-scale measurement wind profiles are divided into wind direction sectors of 10 degrees and are shown in Figs. 14 and 15 for the easterly and westerly winds, respectively. The measured profiles for the mean wind velocity and turbulence intensity from the wind tunnel tests are indicated in the same figures and are divided into easterly and westerly winds, corresponding to the two terrain models described in the previous sections.

Some spanwise nonuniformity in the wind field can be expected for such a bridge, where the surface roughness is smaller in the middle of the fjord than towards each side. A decrease in mean wind velocity, and corresponding increase in turbulence intensity towards the bridge ends would result from such conditions, however the complexity of the surrounding terrain may distort this behavior. From Fig. 14, a quite uniform wind field is displayed for the first 1-3 sectors of the easterly winds, but for sector 4-7 the surface roughness effect described above is becoming increasingly clear. Though no distinct linear trend is observed from the full-scale measured wind profiles for this wind direction, the profiles measured in the wind tunnel terrain model tests display a clear linear variation both for the mean wind velocity and the turbulence intensity, but with an opposite sign of inclination. The variation is stronger in the test configuration with a turbulent inflow than in the smooth inflow case. The easterly wind direction modeled in the wind tunnel is closest to sectors 4-6 in Fig. 14. Although the linear trend from the wind tunnel tests is not observed at the middle part of the span in the full-scale measurements, a similar trend can be observed for the northern part of the bridge. Here, the mean wind speed is decreasing, and the turbulence intensity is increasing, in better correspondence with the wind tunnel profiles.

For the westerly winds, it has previously been noted that the modeled terrain direction does not seem to represent the dominant incoming wind direction very well. The modeled direction corresponds best with sectors 8 and 9 for the full-scale measurements shown in Fig. 15. The wind tunnel experiments show a very homogenous behavior for both the mean wind velocity and the turbulence intensity along the span, in strong contradiction to what can be observed in Fig. 13. However, for sectors 8 and 9, the homogeneity identified by the terrain model wind tunnel tests seem to correspond quite well to the full-scale measurements for the middle part of the span. The A8 sensor closest to the north end of the bridge shows a different behavior, but this behavior could not be captured by the wind tunnel experiments since only the middle part of the bridge span was investigated. For sectors 10 and 11, a linear trend in both the mean wind velocity and the turbulence intensity profiles is observed. This corresponds to the observation made for the turbulence intensity in Fig. 13, but the trend for the mean wind velocity is clearer in Fig. 15 than in Fig. 10. This trend is an illustration of the strong terrain induced effects on the wind field inhomogeneity at this very complex bridge site.

The full-scale turbulence intensities display a large variability, but the turbulence intensity levels from the wind tunnel tests agree quite well with the measured mean value levels for the corresponding sectors of the westerly winds. This is an indication that most of the turbulence is generated locally for this wind direction. For the easterly winds, the full-scale measurements display levels in the area between the two test configurations, indicating that some influence from the incoming flow affects the local turbulence characteristics as well. These observations agree with the initial assumptions about the inflow conditions and indicate that the surface model of the terrain model is performing well.

A few studies have investigated the effects of the homogeneity assumption often used in buffeting calculations (Arena et al., 2014; Hu et al., 2017; Zhang, 2007). Fig. 15 shows turbulence profiles that vary as much as 100% over a length of approximately 900 m and mean wind velocities that vary by approximately 50% over the same length. The Hardanger Bridge site is extremely complex; however, it is quite typical for Norwegian terrain. Other areas of the world where long-span bridges are constructed show similar complexities, such as mountain gorge terrains in China, as investigated by (Li et al., 2010, 2016). In such conditions, extreme nonuniform profiles may be important for both the buffeting action and aerodynamic instability effects of long-span bridges.

One of the main approaches to estimate such nonuniformity in the wind field is by using terrain model wind tunnel tests. In this study, some discrepancies in the tested wind field profiles from the wind tunnel were found when compared with the full-scale measurements. However, some promising results were also found, especially for the uniformity in the westerly wind profiles and the turbulence intensity levels predicted by the wind tunnel experiments. Some of the unsatisfactory results from the wind tunnel tests for the Hardanger Bridge site can be explained by the limited size of the terrain model and the limited number of tested incoming wind directions. A larger scale and a larger modeled area would be expected to increase the performance of the wind tunnel test results for the Hardanger Bridge site.

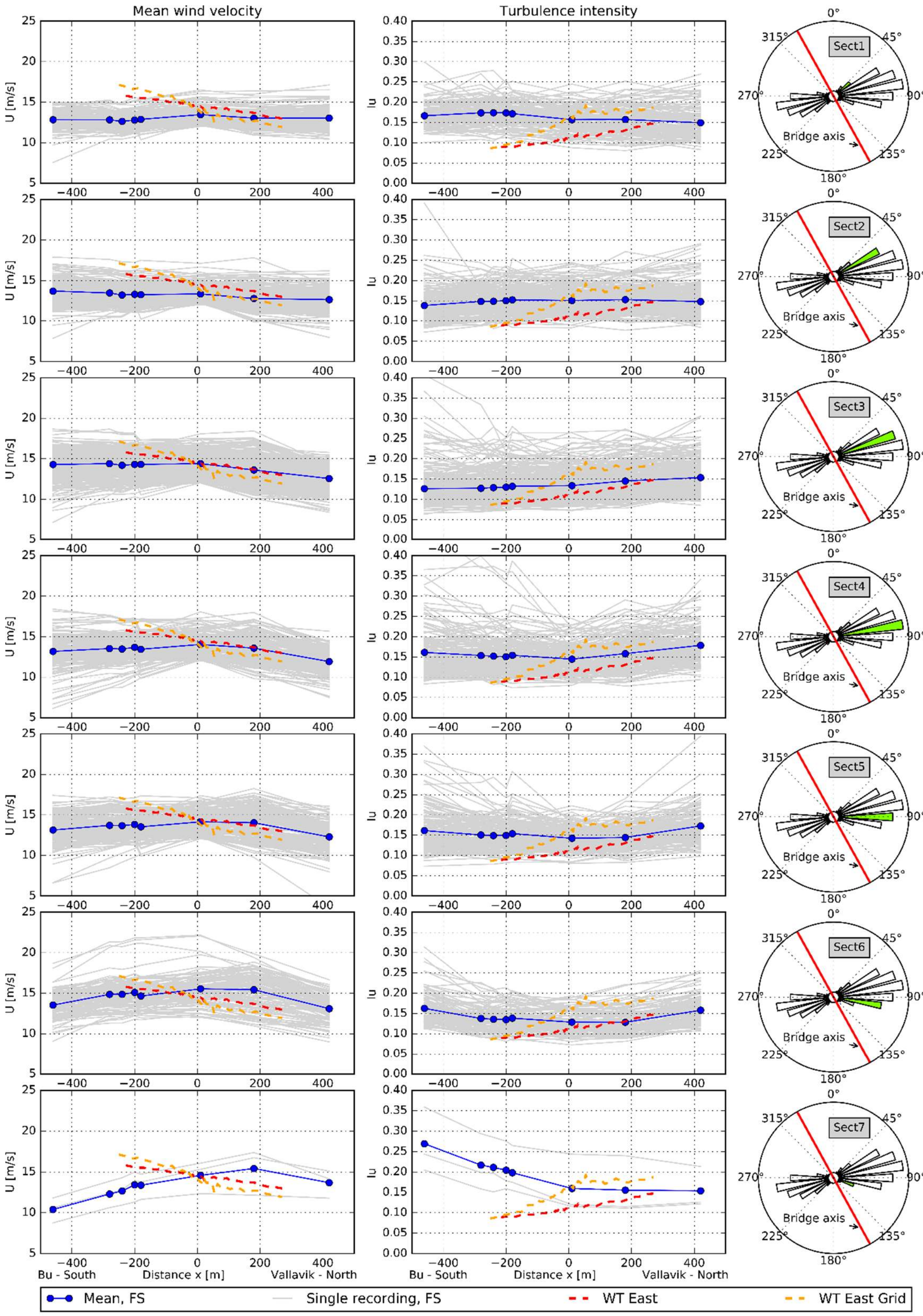

Fig. 14. Along-span simultaneously measured wind field profiles for easterly winds. FS, denotes "Full-scale measurements" and WT denotes "Wind Tunnel tests". On the right side of the figures, midspan (A6) wind rose for the FS profiles are given, highlighting the associated sector for the mean wind direction."

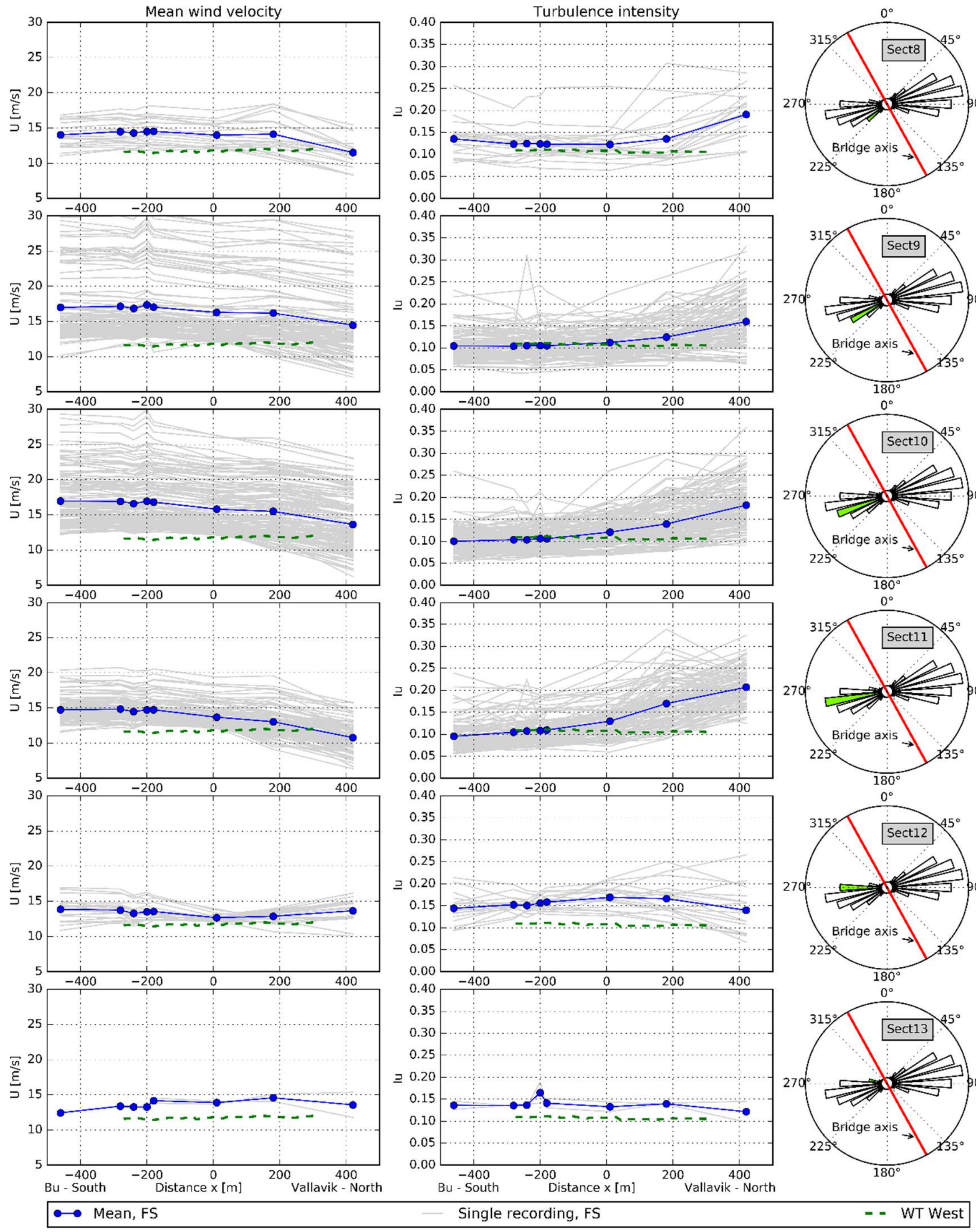

Fig. 15. Along-span simultaneously measured wind field profiles for westerly winds. FS, denotes "Full-scale measurements" and WT denotes "Wind Tunnel tests". On the right side of the figures, midspan (A6) wind rose for the FS profiles are given, highlighting the associated sector for the mean wind direction."

6 Conclusions

The spatial variations in the wind field characteristics at the Hardanger Bridge site have been investigated in this paper. The performance of traditional wind field characterization methods, namely, in situ mast measurements and wind tunnel terrain model experiments, for predicting the wind field along a bridge girder in complex terrain has been studied, and the following conclusions can be drawn:

- The mean wind direction varies along the Hardanger Bridge span indicating terrain-induced effects on the mean wind direction. Caution should be taken when using wind directions measured at a single point as a basis for inflow directions for wind tunnel terrain model tests.
- The easterly wind field was composed of incoming flows from two different fjord arms due to terrain channeling effects.
- Extreme value statistics were used to compare wind speeds between nonsimultaneous measurement campaigns. Local wind speed-up effects measured at the mast location were successfully predicted using the calculation guidelines defined in the European design code for wind actions, despite the limitations of this code regarding complex terrain. The terrain model wind tunnel tests also successfully predicted the speed-up effect for the easterly wind direction but underpredicted the speed-up effect for the westerly winds.
- Turbulence intensity levels measured at the mast were larger than those measured along the bridge span. The larger turbulence intensity measured at the mast can be explained as a combination of flow separation over the hill and local vegetation at the mast location, imposing higher surface roughness. The design guidelines would fail to predict such an effect resulting in an underestimation of the turbulence intensity.
- The probability distribution of the turbulence intensity followed a lognormal probability density function for the mast and for all the along-span anemometers.
- The wind field along the Hardanger Bridge girder displayed spanwise nonuniform behavior for both the mean wind velocity and along-wind turbulence intensity. The turbulence intensities varied up to 100% and the mean wind velocities varied up to 50% along the span.
- The terrain model wind tunnel experiments were unable to adequately predict the spanwise wind profiles for the easterly wind direction, but better agreement was found for the modeled westerly wind directions. This indicates the importance of modeling an appropriately large terrain area and investigating different incoming wind directions.
- In situ mast measurements and terrain model wind tunnel tests as the source of wind field information for design purposes can be a satisfactory method under the following conditions:
    - Special attention should be given to the position of the mast
    - The scale and size of the model need to be large enough to allow the testing of several incoming wind directions.
- Single-point mast measurements should be complemented by additional masts, terrain model tests or LIDARs to more accurately capture the spatial transfer.

7 Acknowledgments

Funding: The research presented in this paper has been financed by the Norwegian Public Roads Administration (NPRA), the Norwegian Research Council and Norconsult.

The authors also thank the NPRA for providing the mast measurement results used in this study.

8 References

Arena, A., Lacarbonara, W., Valentine, D.T., Marzocca, P., 2014. Aeroelastic behavior of long-span suspension bridges under arbitrary wind profiles. J. Fluids Struct. 50, 105–119. https://doi.org/10.1016/j.jfluidstructs.2014.06.018

Balakrishnan, N., Chan, P.S., 1992. Order statistics from extreme value distribution, ii: Best linear unbiased estimates and some other uses. Commun. Stat. - Simul. Comput. 21, 1219–1246. https://doi.org/10.1080/03610919208813074

Bietry, J., Delaunay, D., Conti, E., 1995. Comparison of full-scale measurement and computation of wind effects on a cable-stayed bridge. J. Wind Eng. Ind. Aerodyn. 57, 225–235. https://doi.org/10.1016/0167-6105(94)00110-Y

Bocciolone, M., Cheli, F., Curami, A., Zasso, A., 1992. Wind measurements on the humber bridge and numerical simulations. J. Wind Eng. Ind. Aerodyn. 42, 1393–1404. https://doi.org/10.1016/0167-6105(92)90147-3

Bowen, A.J., 2003. Modelling of strong wind flows over complex terrain at small geometric scales. J. Wind Eng. Ind. Aerodyn. 91, 1859–1871. https://doi.org/10.1016/j.jweia.2003.09.029

Brownjohn, J.M.W., Bocciolone, M., Curami, A., Falco, M., Zasso, A., 1994. Humber bridge full-scale measurement campaigns 1990–1991. J. Wind Eng. Ind. Aerodyn. 52, 185–218. https://doi.org/10.1016/0167-6105(94)90047-7

Burlando, M., De Gaetano, P., Pizzo, M., Repetto, M.P., Solari, G., Tizzi, M., 2013. Wind climate analysis in complex terrains. J. Wind Eng. Ind. Aerodyn. 123, 349–362. https://doi.org/10.1016/j.jweia.2013.09.016

Cao, S., Tamura, Y., Kikuchi, N., Saito, M., Nakayama, I., Matsuzaki, Y., 2009. Wind characteristics of a strong typhoon. J. Wind Eng. Ind. Aerodyn. 97, 11–21. https://doi.org/10.1016/J.JWEIA.2008.10.002

Carpenter, P., Locke, N., 1999. Investigation of wind speeds over multiple two-dimensional hills. J. Wind Eng. Ind. Aerodyn. 83, 109–120. https://doi.org/10.1016/S0167-6105(99)00065-3

Cheynet, E., Bogunovic Jakobsen, J., Snæbjörnsson, J., 2016. Buffeting response of a suspension bridge in complex terrain. Eng. Struct. 128, 474–487. https://doi.org/10.1016/J.ENGSTRUCT.2016.09.060

Choi, E.C.C., 1978. Characteristics of typhoons over the South China Sea. J. Wind Eng. Ind. Aerodyn. 3, 353–365. https://doi.org/10.1016/0167-6105(78)90038-7

Ciampoli, M., Petrini, F., Augusti, G., 2011. Performance-Based Wind Engineering: Towards a general procedure. Struct. Saf. 33, 367–378. https://doi.org/10.1016/J.STRUSAFE.2011.07.001

Cook, N.J., 1982. Towards better estimation of extreme winds. J. Wind Eng. Ind. Aerodyn. 9, 295–323.

Cook, N.J., Harris, R.I., 2008. Postscript to "Exact and general FT1 penultimate distributions of extreme wind speeds drawn from tail-equivalent Weibull parents." Struct. Saf. 30, 1–10. https://doi.org/10.1016/J.STRUSAFE.2006.04.001

Cook, N.J., Harris, R.I., 2004. Exact and general FT1 penultimate distributions of extreme wind speeds drawn from tail-equivalent Weibull parents. Struct. Saf. 26, 391–420. https://doi.org/10.1016/J.STRUSAFE.2004.01.002

Cross, E.J., Koo, K.Y., Brownjohn, J.M.., Worden, K., 2013. Long-term monitoring and data analysis of the Tamar Bridge. Mech. Syst. Signal Process. 35, 16–34. https://doi.org/10.1016/J.YMSSP.2012.08.026

Davenport, A.G., 1983. The relationship of reliability to wind loading. J. Wind Eng. Ind. Aerodyn. 13, 3–27. https://doi.org/10.1016/0167-6105(83)90125-3

Davenport, A.G., 1962. Buffeting of a suspension bridge by storm winds. J. Struct. Div. 88, 233–270.

Fenerci, A., Øiseth, O., 2018. Strong wind characteristics and dynamic response of a long-span suspension bridge during a storm. J. Wind Eng. Ind. Aerodyn. 172, 116–138.

Fenerci, A., Øiseth, O., 2017. Measured buffeting response of a long-span suspension bridge compared with numerical predictions based on design wind spectra. J. Struct. Eng. 143.

Fenerci, A., Øiseth, O., Rönnquist, A., 2017. Long-term monitoring of wind field characteristics and dynamic response of a long-span suspension bridge in complex terrain. Eng. Struct.

Gumbel, E.J., 1958. Statistics of extremes. Columbia University Press, New York.

Harris, R.I., 2009. XIMIS, a penultimate extreme value method suitable for all types of wind climate. J. Wind Eng. Ind. Aerodyn. 97, 271–286. https://doi.org/10.1016/J.JWEIA.2009.06.011

Harris, R.I., 1999. Improvements to the `Method of Independent Storms'. J. Wind Eng. Ind. Aerodyn. 80, 1–30. https://doi.org/10.1016/S0167-6105(98)00123-8

Harris, R.I., 1996. Gumbel re-visited - A new look at extreme value statistics applied to wind speeds. J. Wind Eng. Ind. Aerodyn. 59, 1–22. https://doi.org/10.1016/0167-6105(95)00029-1

Harstveit, K., 1996. Full scale measurements of gust factors and turbulence intensity, and their relations in hilly terrain. J. Wind Eng. Ind. Aerodyn. 61, 195–205. https://doi.org/10.1016/0167-6105(96)00047-5

Harstveit, K., 1994. Hardangerbrua - Sluttrapport for vindmålinger 32/93 KLIMA.

Hu, L., Xu, Y.-L., Huang, W.-F., 2013. Typhoon-induced non-stationary buffeting response of long-span bridges in complex terrain. Eng. Struct. 57, 406–415. https://doi.org/10.1016/J.ENGSTRUCT.2013.09.044

Hu, L., Xu, Y., Zhu, Q., Guo, A., Kareem, A., 2017. Tropical Storm – Induced Buffeting Response of Long-Span Bridges : Enhanced Nonstationary Buffeting Force Model. J. Struct. Eng. 143, 4017027. https://doi.org/10.1061/(ASCE)ST.1943-541X.0001745.

Hui, M.C.H., Larsen, A., Xiang, H.F., 2009a. Wind turbulence characteristics study at the Stonecutters

Bridge site: Part II: Wind power spectra, integral length scales and coherences. J. Wind Eng. Ind. Aerodyn. 97, 48–59. https://doi.org/10.1016/j.jweia.2008.11.003

Hui, M.C.H., Larsen, A., Xiang, H.F., 2009b. Wind turbulence characteristics study at the Stonecutters Bridge site: Part I-Mean wind and turbulence intensities. J. Wind Eng. Ind. Aerodyn. 97, 22–36. https://doi.org/10.1016/j.jweia.2008.11.002

Ian Harris, R., 2014. A simulation method for the macro-meteorological wind speed and the implications for extreme value analysis. J. Wind Eng. Ind. Aerodyn. 125, 146–155. https://doi.org/10.1016/J.JWEIA.2013.12.003

Kareem, A., 1988. Aerodynamic response of structures with parametric uncertainties. Struct. Saf. 5, 205–225. https://doi.org/10.1016/0167-4730(88)90010-0

Li, C.G., Chen, Z.Q., Zhang, Z.T., Cheung, J.C.K., 2010. Wind tunnel modeling of flow over mountainous valley terrain. Wind Struct. An Int. J. 13, 275–292. https://doi.org/10.12989/was.2010.13.3.275

Li, L., Kareem, A., Xiao, Y., Song, L., Zhou, C., 2015. A comparative study of field measurements of the turbulence characteristics of typhoon and hurricane winds. J. Wind Eng. Ind. Aerodyn. 140, 49–66. https://doi.org/10.1016/J.JWEIA.2014.12.008

Li, Y., Hu, P., Xu, X., Qiu, J., 2016. Wind characteristics at bridge site in a deep-cutting gorge by wind tunnel test. Jnl. Wind Eng. Ind. Aerodyn. 160, 30–46. https://doi.org/10.1016/j.jweia.2016.11.002

Lieblein, J., 1974. Efficient methods of extreme-value methodology. Washington D. C.

Lystad, T.M., Fenerci, A., Sætran, L., Øiseth, O., 2017. Wind field characteristics at the Hardanger Bridge site: Comparison of wind tunnel terrain mode tests with full-scale measurements, in: European-African Conference on Wind Engineering.

Macdonald, J.H.G., 2003. Evaluation of buffeting predictions of a cable-stayed bridge from full-scale measurements. J. Wind Eng. Ind. Aerodyn. 91, 1465–1483. https://doi.org/10.1016/J.JWEIA.2003.09.009

Meroney, R.N., 1980. Wind-tunnel simulation of the flow over hills and complex terrain. J. Wind Eng. Ind. Aerodyn. 5, 297–321. https://doi.org/10.1016/0167-6105(80)90039-2

Miller, C.A., Davenport, A.G., 1998. Guidelines for the calculation of wind speed-ups in complex terrain. J. Wind Eng. Ind. Aerodyn. 74–76, 189–197. https://doi.org/10.1016/S0167-6105(98)00016-6

Miyata, T., Yamada, H., Katsuchi, H., Kitagawa, M., 2002. Full-scale measurement of Akashi–Kaikyo Bridge during typhoon. J. Wind Eng. Ind. Aerodyn. 90, 1517–1527. https://doi.org/10.1016/S0167-6105(02)00267-2

Pagnini, L., 2010. Reliability analysis of wind-excited structures. J. Wind Eng. Ind. Aerodyn. 98, 1–9. https://doi.org/10.1016/J.JWEIA.2009.08.010

Pagnini, L.C., Solari, G., 2002. Gust buffeting and turbulence uncertainties. J. Wind Eng. Ind. Aerodyn. 90, 441–459. https://doi.org/10.1016/S0167-6105(01)00202-1

Scanlan, R.H., 1978a. The action of flexible bridges under wind, I: Flutter theory. J. Sound Vib. 60, 187–199. https://doi.org/10.1016/S0022-460X(78)80028-5

Scanlan, R.H., 1978b. The action of flexible bridges under wind, II: Buffeting theory. J. Sound Vib. 60, 201–211. https://doi.org/10.1016/S0022-460X(78)80029-7

Scanlan, R.H., Tomko, J.J., 1971. Airfoil and bridge deck flutter derivatives. J. Eng. Mech. Div. 97, 1717–1737.

Solari, G., 1997. Wind-excited response of structures with uncertain parameters. Probabilistic Eng. Mech. 12, 75–87. https://doi.org/10.1016/S0266-8920(96)00027-6

Spence, S.M.J., Kareem, A., 2014. Performance-based design and optimization of uncertain wind-excited dynamic building systems. Eng. Struct. 78, 133–144. https://doi.org/10.1016/J.ENGSTRUCT.2014.07.026

Standard Norge, 2009. Eorocode 1: Actions on structures - Part 1-4: General actions, Wind actions.

Stevenson, D.C., Lindley, D., Neal, D., Zealand, N., House, T., Kingdom, U., 1981. A wind tunnel boundary-layer simulation of wind flow over complex terrain: Effect of terrain and model construction 21, 271–293.

Sætran, L.R., Malvik, I.M., 1991. Hardangerbrua - Vindteknisk undersøkelse av terrengmodell i vindtunnel.

Tamura, Y., Kareem, A., 2013. Advanced Structural Wind Engineering. Springer Japan.

Torrielli, A., Repetto, M.P., Solari, G., 2013. Extreme wind speeds from long-term synthetic records. J. Wind Eng. Ind. Aerodyn. 115, 22–38. https://doi.org/10.1016/J.JWEIA.2012.12.008

Wang, H., Hu, R., Xie, J., Tong, T., Li, A., 2013. Comparative study on buffeting performance of Sutong Bridge based on design and measured spectrum. J. Bridg. Eng. 18, 587–600. https://doi.org/10.1061/(ASCE)BE.1943-5592.0000394

Wang, H., Li, A., Guo, T., Xie, J., 2009. Field measurement on wind characteristic and buffeting response of the Runyang Suspension Bridge during typhoon Matsa. Sci. China, Ser. E Technol. Sci. 52, 1354–1362. https://doi.org/10.1007/s11431-008-0238-y

Wang, H., Li, A., Hu, R., 2011. Comparison of Ambient Vibration Response of the Runyang Suspension Bridge under Skew Winds with Time-Domain Numerical Predictions. J. Bridg. Eng. 16, 513. https://doi.org/10.1061/(ASCE)BE.1943-5592.0000168

Wang, X., Chen, B., Sun, D., Wu, Y., 2014. Study on typhoon characteristic based on bridge health monitoring system. Sci. World J. 2014. https://doi.org/10.1155/2014/204675

Wang, X., Huang, P., Yu, X.-F., Wang, X.-R., Liu, H.-M., 2017. Wind characteristics near the ground during typhoon Meari. J. Zhejiang Univ. Sci. A 18, 33–48. https://doi.org/10.1631/jzus.A1500310

Xu, Y.-L., 2013. Wind effects on cable-supported bridges. Wiley, Hong Kong.

Xu, Y., Øiseth, O., Naess, A., Moan, T., 2017. Prediction of long-term extreme load effects due to wind for cable-supported bridges using time-domain simulations. Eng. Struct. 148, 239–253. https://doi.org/10.1016/J.ENGSTRUCT.2017.06.051

Zhang, L., Li, J., Peng, Y., 2008. Dynamic response and reliability analysis of tall buildings subject to wind loading. J. Wind Eng. Ind. Aerodyn. 96, 25–40. https://doi.org/10.1016/J.JWEIA.2007.03.001

Zhang, X., 2007. Influence of some factors on the aerodynamic behavior of long-span suspension bridges. J. Wind Eng. Ind. Aerodyn. 95, 149–164. https://doi.org/10.1016/J.JWEIA.2006.08.003